Biomimatic material(생체 모방 재료)의 센서 응용에 대한 연구동향

Chung-Ang University, Da Vinci College of General Education
OK JA Yoon

CHERIC
Chemical Engineering and Materials Research Information Center
국가지정
화학공학소재연구정보센터

연구 동향

✓ **Biomimetic Tactile Sensors with Bilayer Fingerprint Ridges Demonstrating Texture Recognition[1]**

- 인간 표피의 지문 융선(human epidermal fingerprint ridges)과 표피(epidermis)를 모방한 표면 운동 인터페이스 (surface kinetic interface, SKIN)를 가지는 생체모방 촉각 센서 (biomimetic tactile sensor)를 개발함.

- SKIN는 elastic moduli로 이루어진 이중 층의 폴리머 구조로 이루어졌으며, 단단한 표피 지문 융선과 부드러운 표피 보드를 사용하여 SKIN의 촉각 감도를 개선했음.

- SKIN 층으로 된 생체 모방 촉각 센서는 20μm 높이 차이를 가지고 있으며 100μm 미만의 표면 구조에 대한 검출 능력을 입증함. 일상 생활에서 쉽게 접근 할 수 있는 텍스처 인공 손가락과 로봇 손가락이 텍스처 인식에 사용될 수 있음을 보여주고 있음.

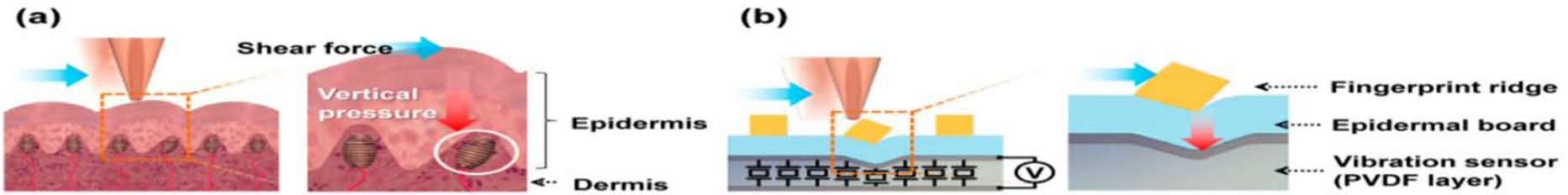

Figure 1. Schematic illustration and shear detecting mechanism of (a) the human fingertip and (b) the biomimetic tactile sensor.

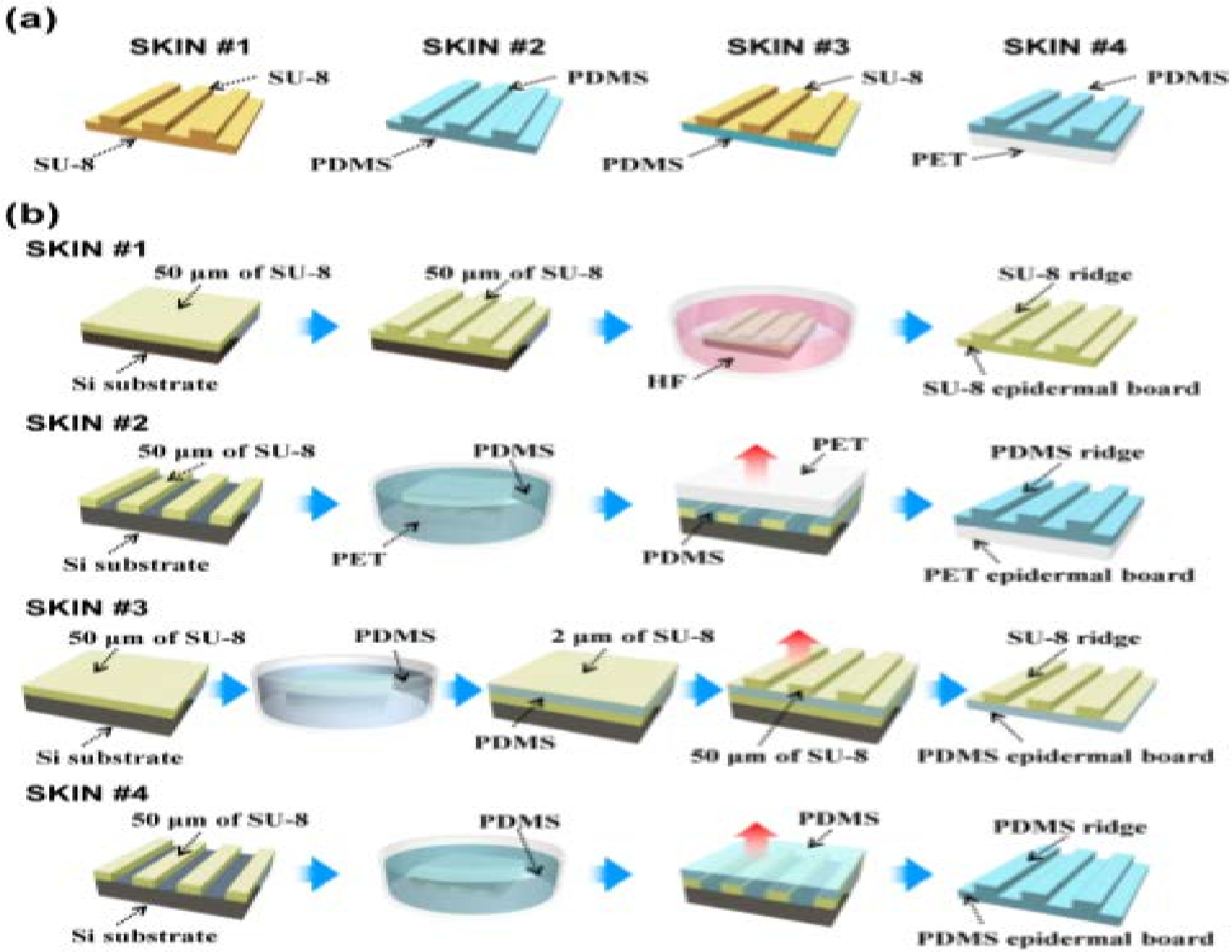

Figure 2. (a) Four types of surface kinetic interfaces (SKINs) with differing mechanical configurations and (b) their fabrication processes.

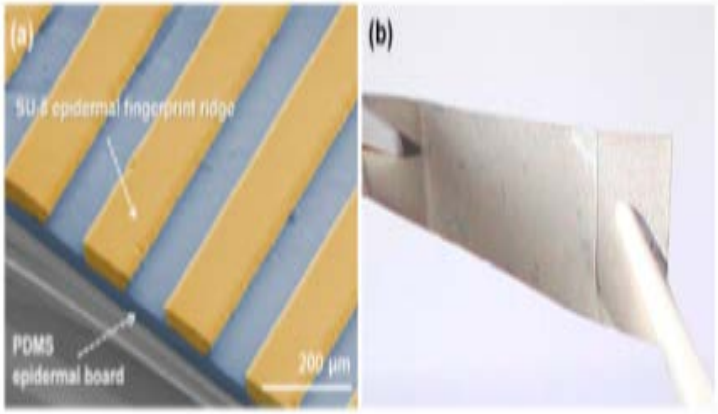

Figure 3. Images of a fabricated biomimetic tactile sensor with SKIN: (**a**) a false-color SEM image of the fabricated SKIN #3, which was composed of (yellow) SU-8 epidermal fingerprint ridges with a 200-μm-period and a 50-μm height, and a (blue) polydimethylsiloxane (PDMS) epidermal board with a 50-μm thickness; (**b**) an optical image of the fabricated flexible biomimetic tactile sensor with SKIN.

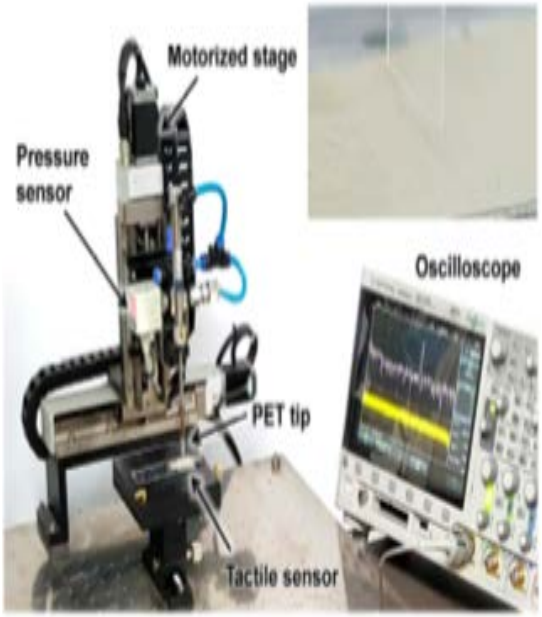

Figure 4. Optical image of the measurement set-up, where the inset shows an optical image of a SKIN and a hovering polyethylene terephthalate (PET) tip.

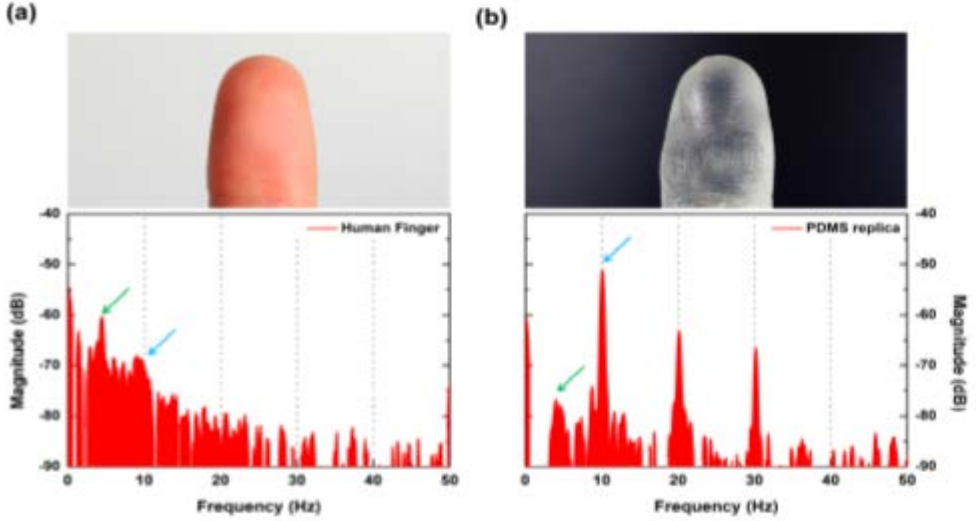

Figure 9. FFT results of tactile sensor output induced by scanning (**a**) a human finger and (**b**) a PDMS replica, where the insets show optical images of a human finger pad and the PDMS replica. Blue arrows indicate the f_{ER}, and green arrows indicate the peaks of ERs of the contact objects.

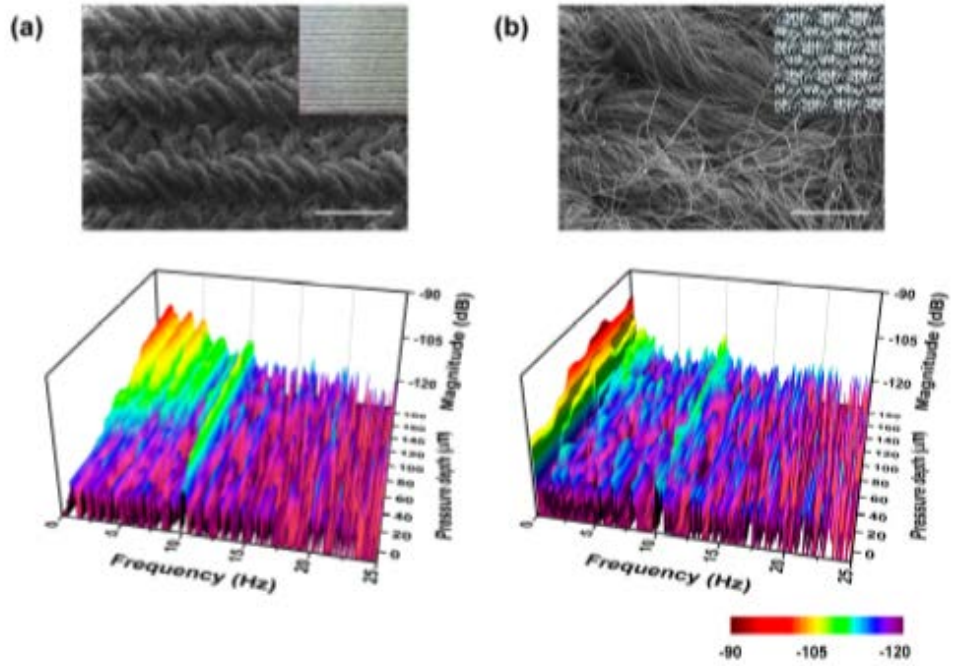

Figure 11. FFT results of tactile sensor output induced by scanning (**a**) a hard fabric with tight weaves and (**b**) a soft fabric with hair-like structures, increasing the contact depth. Inset images show SEM and optical images of the two different fabrics (scale bars indicate 1 mm).

✓ Ti-Catalyst Biomimetic Sensor for the Detection of Nitroaromatic Pollutants[2]

- 나피온에 Ti 촉매 농도를 최적화하여 섞은 용액을 전극에 코팅하여 니트로 방향족 화합물 (nitro-aromatic compounds, NAC)의 전기 화학적 특성을 검출하기 위한 센서 개발을 보고하고 있음.

- Ti 촉매로 코팅된 전극은 니트로 종(nitro species)의 검출에서 높은 안정성을 보였으며 농도에 따라 다른 28개의 다른 코팅 전극의 검출을 분석한 결과 약 15%의 표준 편차를 입증함.

- Ti 촉매로 코팅된 전극으로 니트로페놀 (nitrophenols), 모노니트로아닐린 (mononitroaniline), 디니트로톨루엔 (dinitrotoluene)과 같은 여러 니트로 방향족 화합물을 검출한 결과 검출 한계가 $1 \times 10^{-4} \sim 9 \times 10^{-4}$ g L^{-1} ($0.2 \times 10^{-6} \sim 5.1 \times 10^{-6}$ mol L^{-1})임을 확인하였고, 티타노센 (titanocene)이 니트로 지방족 화합물의 환원을 촉매하지 않기 때문에 NAC 검출에 대한 우수한 선택성을 보임을 보고함.

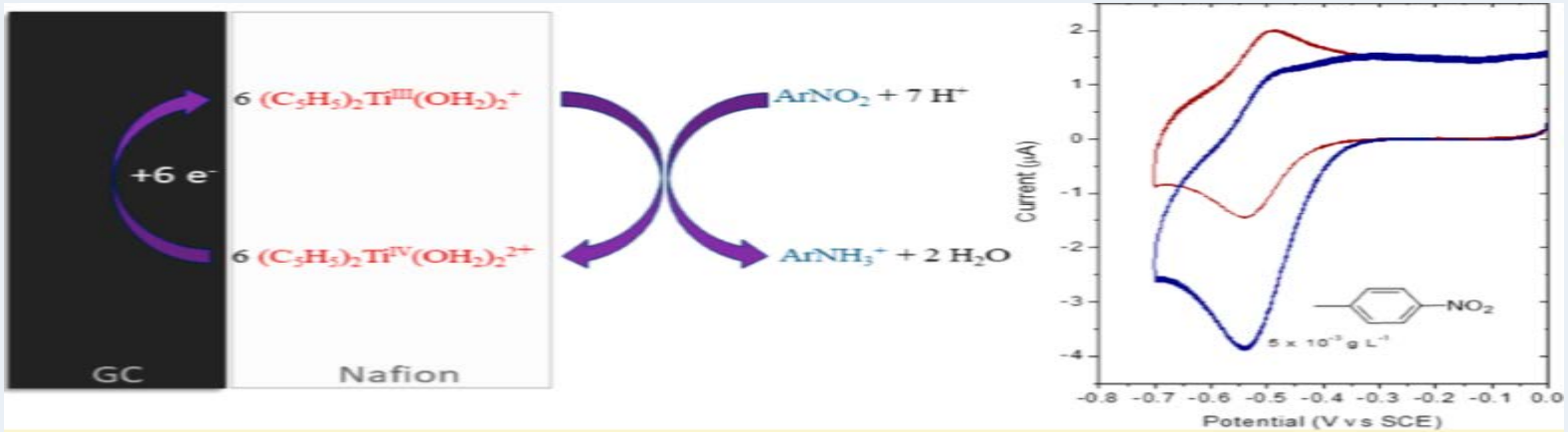

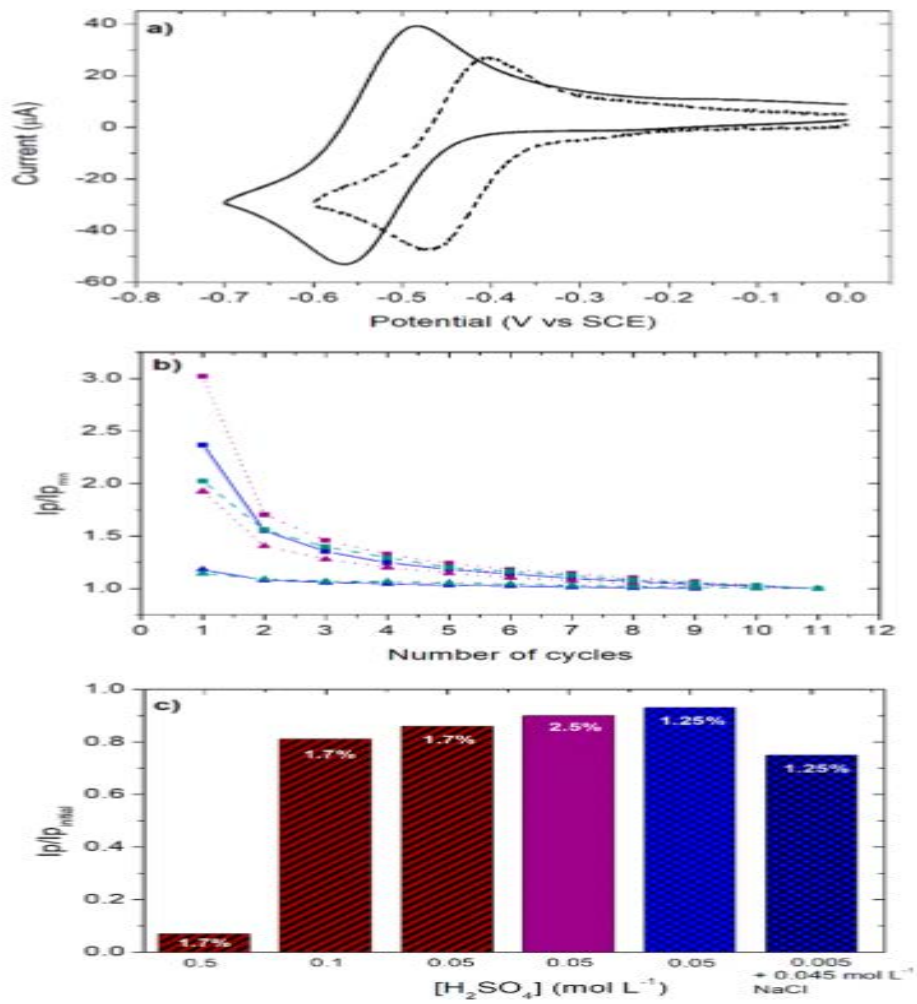

Figure 1. (a) Cyclic voltammograms of the titanocene complex (4×10^{-3} mol L^{-1}) on the glassy-carbon electrode (3 mm in diameter) in 0.5 mol L^{-1} H_2SO_4 (dotted line) and on the Nafion-modified electrode ([Nafion] = 2.5% and [$(C_5H_5)_2TiCl_2$] = 4×10^{-3} mol L^{-1}, 11th scan) in 0.05 mol L^{-1} H_2SO_4 (solid line). Scan rate: 100 mV s^{-1}. (b) Reduction-peak current, I_p, normalized to the reduction-peak current after stabilization, $I_{p_{min}}$, vs the number of cycles obtained in cyclic voltammetry for the titanocene-modified electrodes prepared with solutions of 2×10^{-4} mol L^{-1} titanocene and 1.25 (—, blue), 2.5 (— —, green), or 3.75% (· · ·, purple) Nafion. The analysis was performed with a newly modified electrode (■) and after the first stabilization using 11 cycles (▲). (c) Reduction-peak current, I_p, normalized to the initial reduction-peak current vs the H_2SO_4 electrolyte concentration, $I_{p_{initial}}$, obtained in cyclic voltammetry after 60 min of immersion of the titanocene-modified electrodes prepared with solutions of 1.3 g L^{-1} (5.2×10^{-3} mol L^{-1}, hatched red bars), 1 g L^{-1} (4.0×10^{-3} mol L^{-1}, plain pink bar), and 0.05 g L^{-1} (2.0×10^{-4} mol L^{-1}, cross-hatched blue bars) titanocene. Nafion concentrations are indicated.

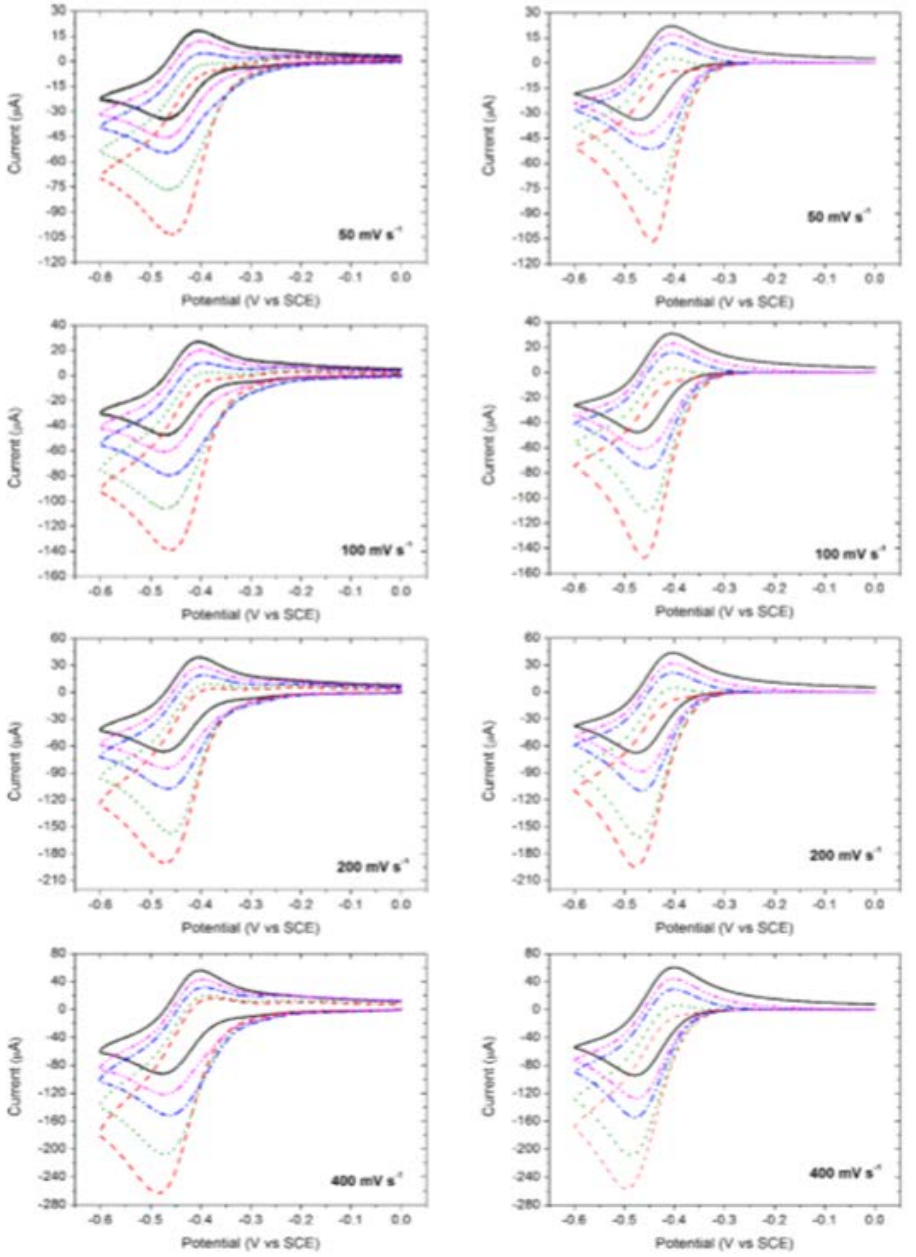

Figure 2. Cyclic voltammograms of titanocene (1 g L^{-1}, 4×10^{-3} mol L^{-1}) in 0.5 mol L^{-1} H_2SO_4 before (—, black) and after the addition of 2.8×10^{-4} (– · · –, pink), 5.5×10^{-4} (– · –, blue), 1.1×10^{-3} (· · ·, green), and 1.6×10^{-3} mol L^{-1} (– – –, red) 4-nitrophenylacetic acid on a 3 mm diameter glassy-carbon electrode (left). Voltammogram simulations considering all the reduction steps after the first one as being fast with $k_1 = 1.9 \times 10^4$ mol^{-1} L s^{-1} (right). The background was subtracted.

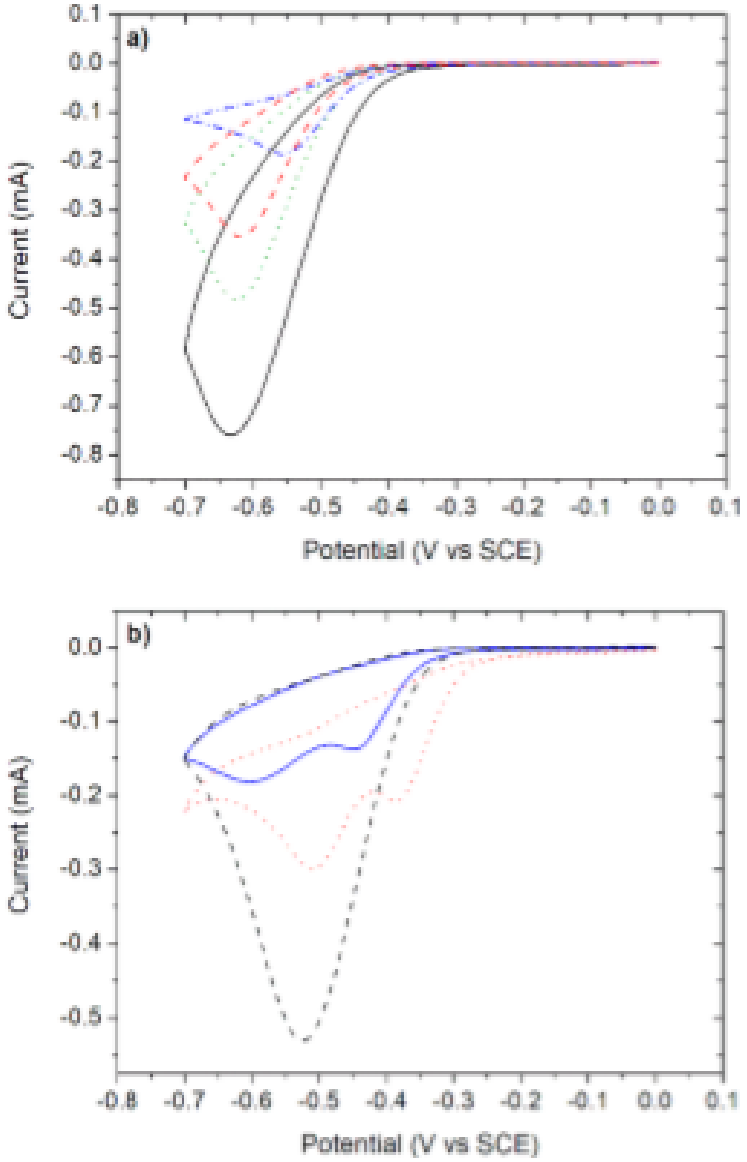

Figure 5. Cyclic voltammograms, in 0.05 mol L^{-1} H_2SO_4 on Nafion-coated electrodes ([Nafion] = 1.25%, 3 mm in diameter), of (a) 0.5 g L^{-1} *m*-nitrophenol (– · – · –, blue), *p*-nitrotoluene (– – –, red), nitrobenzene (· · ·, green), and *m*-nitroaniline (—, black) and of (b) 0.5 g L^{-1} 2,4-dinitrotoluene (—, blue), metronidazole (· · ·, red), and 2,6-dinitrophenol (– – –, black). Scan rate: 100 mV s^{-1}.

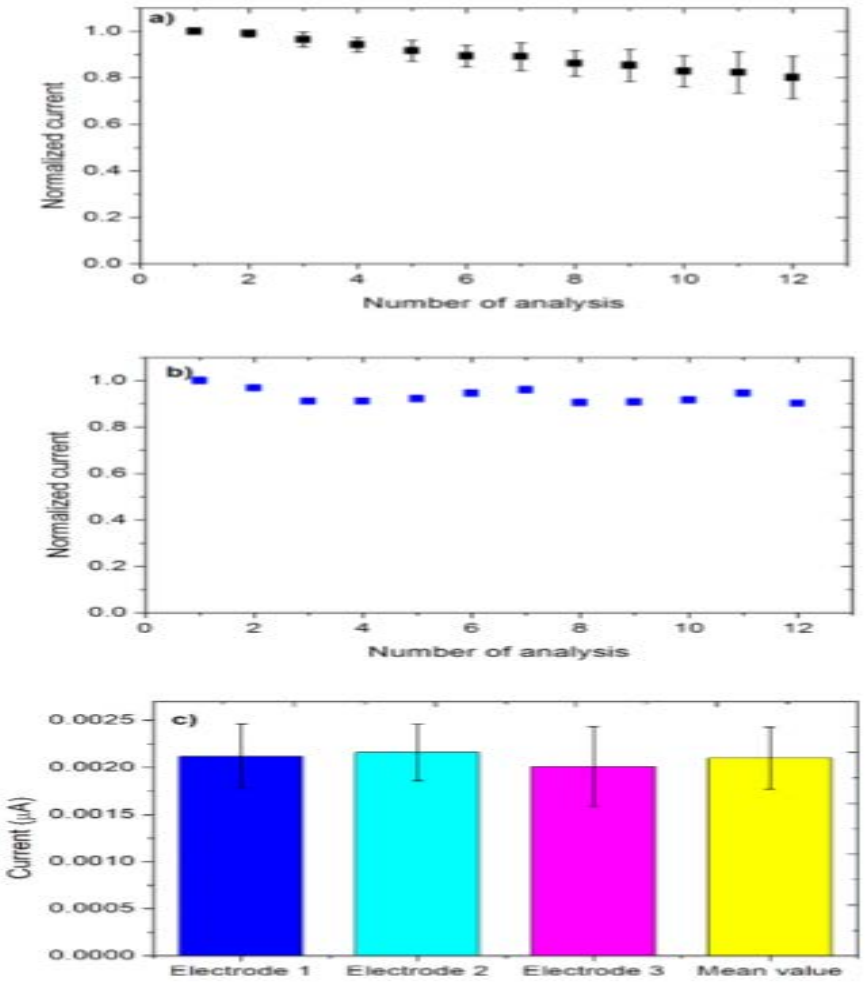

Figure 4. (a) Oxidation-peak current measured by cyclic voltammetry in 0.05 mol L^{-1} H_2SO_4 and normalized by the signal of the first analysis after stabilization of the $(C_5H_5)_2Ti^{IV}(OH_2)_2^{2+}$-modified electrode ([Nafion] = 1.25% and $[(C_5H_5)_2TiCl_2] = 8 \times 10^{-5}$ mol L^{-1}). Error bars are based on the electrochemical signals given by nine different modified electrodes. (b) Reduction-peak currents measured by cyclic voltammetry in 0.05 mol L^{-1} H_2SO_4 and normalized according to the first analysis after stabilization of the $(C_5H_5)_2Ti^{IV}(OH_2)_2^{2+}$-modified electrode ([Nafion] = 1.25% and $[(C_5H_5)_2TiCl_2] = 8 \times 10^{-5}$ mol L^{-1}) and after addition of a 5.5×10^{-5} mol L^{-1} solution of 4-nitrophenylacetic acid. Scan rate: 100 mV s^{-1}. (c) Mean values of the maximum reduction-peak-current responses measured by cyclic voltammetry in 0.05 mol L^{-1} H_2SO_4 (second cycle) of 28 different $(C_5H_5)_2Ti^{IV}(OH_2)_2^{2+}$-modified electrodes ([Nafion] = 1.25% and $[(C_5H_5)_2TiCl_2] = 8 \times 10^{-5}$ mol L^{-1}): 10 responses from electrode 1 and 9 responses each from electrodes 2 and 3. A mean value taking into account all 28 data points is also given.

✓ Electrochemical sensors based on biomimetic magnetic molecularly imprinted polymer for selective quantification of methyl green in environmental samples[3]

- 메틸 그린 염료 (methyl green dye)를 모니터링하고 높은 민감도와 선택적인 검출을 위해 magnetic molecularly imprinted polymer (mag-MIP)를 탄소 페이스트 전극 (carbon paste electrode)에 코팅하여 새로운 생체 모방 센서를 제조함.

- Pseudo-first order kinetics 모델링에 의해 mag-MIP 위에서의 염료 maximum adsorption (Qm)은 3.13 mg g^{-1}이고, 비교군으로 magnetic non-imprinted polymer (mag-NIP)을 제조하였으며 Qm의 값은 1.58 mg g^{-1}임을 보고함.

- 전기 화학적 분석을 통해, 1.0 × 10^{-8} mol L^{-1} 검출 한계 (LOD), 9.9 × 10^{-10} ~ 8 × 10^{-6} mol L^{-1}의 선형 농도 범위 (linear concentration range), 4.3 %의 상대 표준 편차 (RSD) (n = 15)인 최적화된 결과를 보고함.

- 개발된 센서는 메틸 그린의 선택적 결합에 의해 93%에서 103% 범위의 회수율의 결과를 얻음으로써 우수한 정밀도와 높은 신뢰성을 입증하였고 실제 샘플에서 메틸 그린의 정량화를 위한 대체 방법의 가능성을 입증하였음.

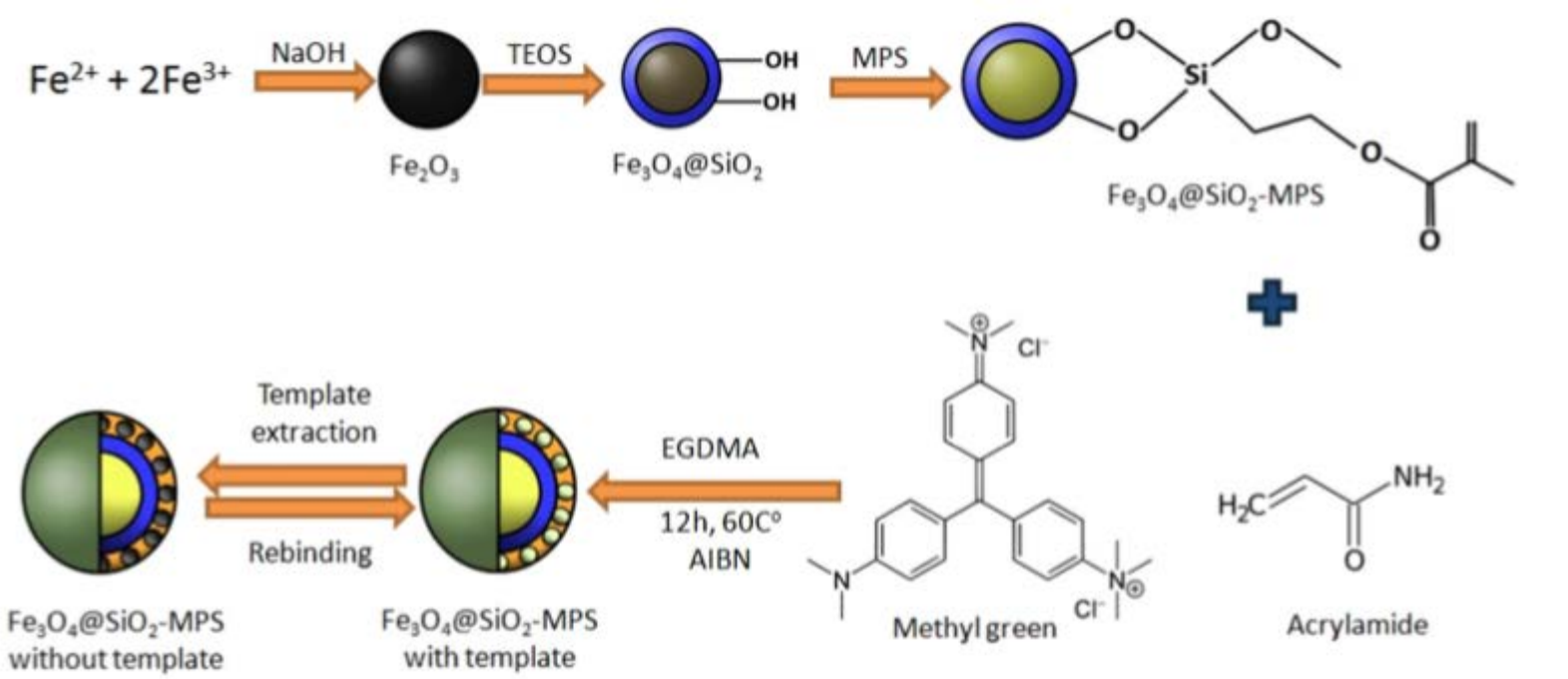

Fig. 1. Schematic representation of all the steps employed in the synthesis of the mag-MIP.

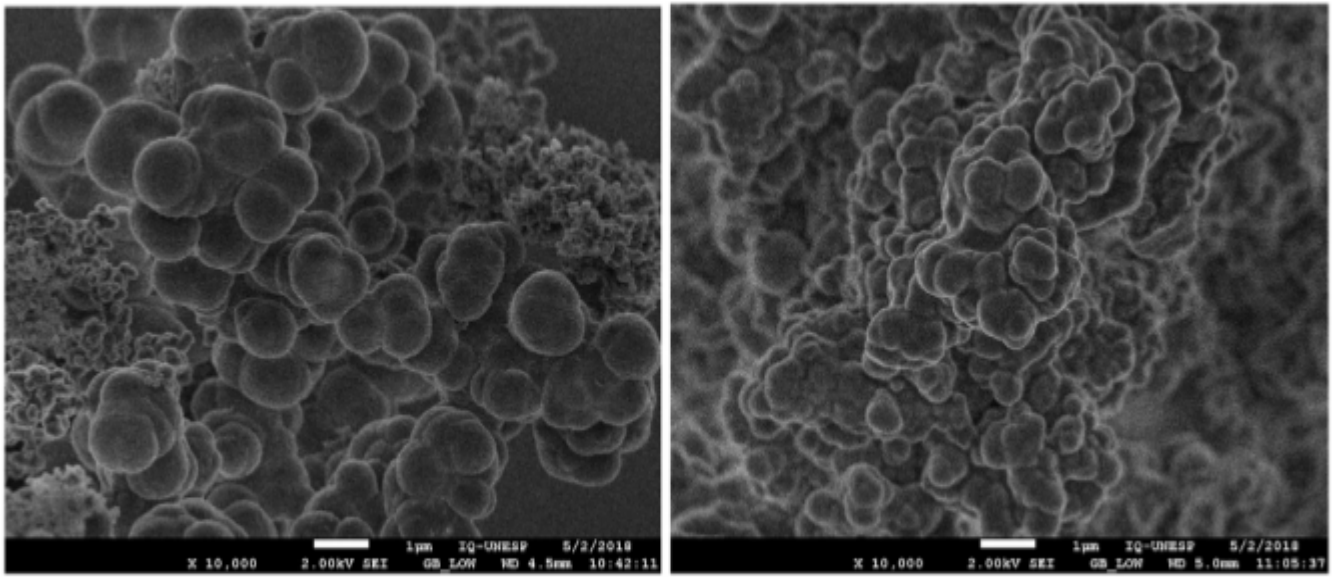

Fig. 2. SEM images of the (A) mag-MIP and (B) mag-NIP materials formed via acrylamide as a functional monomer. Scale bar: 1 μm.

✓ Biomimetic magnetic sensor for electrochemical determination of scombrotoxin in fish[4]

- Mmagnetic molecularly imprinted polymer (magnetic-MIP)기반으로 만들어진 센서를 이용하여 어류의 scombrotoxin (histamine)을 검출하는 전기화학적 센싱을 위한 연구 결과로 빠른 센싱과 저가 비용의 센서개발을 보고함.

- Histamine magnetic-MIP 는 core-shell method 로 histamine 을 코어 tamplate로 사용하였고 기능성 monomer로 2-vinyl pyridine을 사용하여 만들었음. MIPs의 장점을 가지고 있는 생체 모방 재료와 자성 입자 (MP)는 낮은 생산 비용, 안정성, 높은 결합력을 가지고 있어 자석의 도움으로 쉽게 분리할 수 있음을 입증함.

- Magnetic-MIP는 어류시료로부터 농축된 히스타민의 전기 화학적 검출을 위해 magneto-actuated electrodes에 직접화시킨 결과 어류 부패 지수 (fish spoilage)가 50 mg kg^{-1}보다 훨씬 낮고 LOD가 1.6 x 10^{-6} mg L^{-1} 정도로 낮은 측정값을 보고함으로써 일상적인 식품 검사에 쉽게 적용할 수 있음을 확인함.

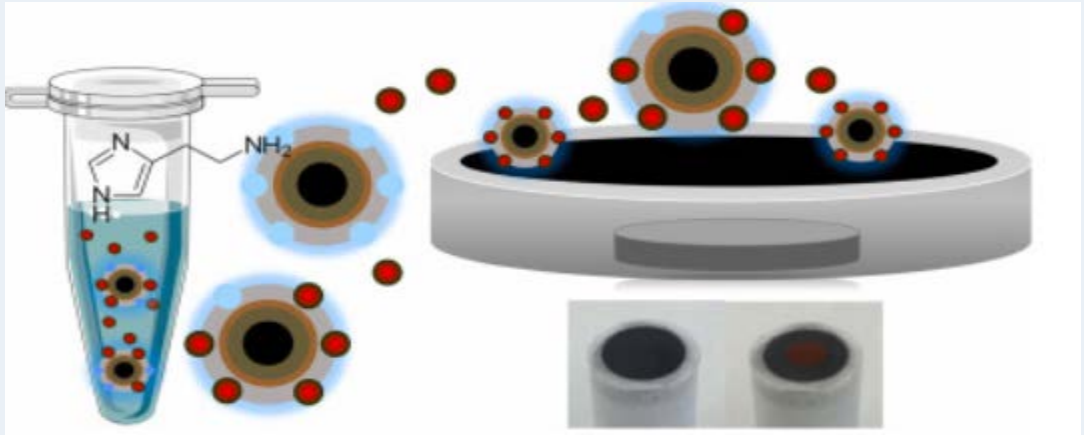

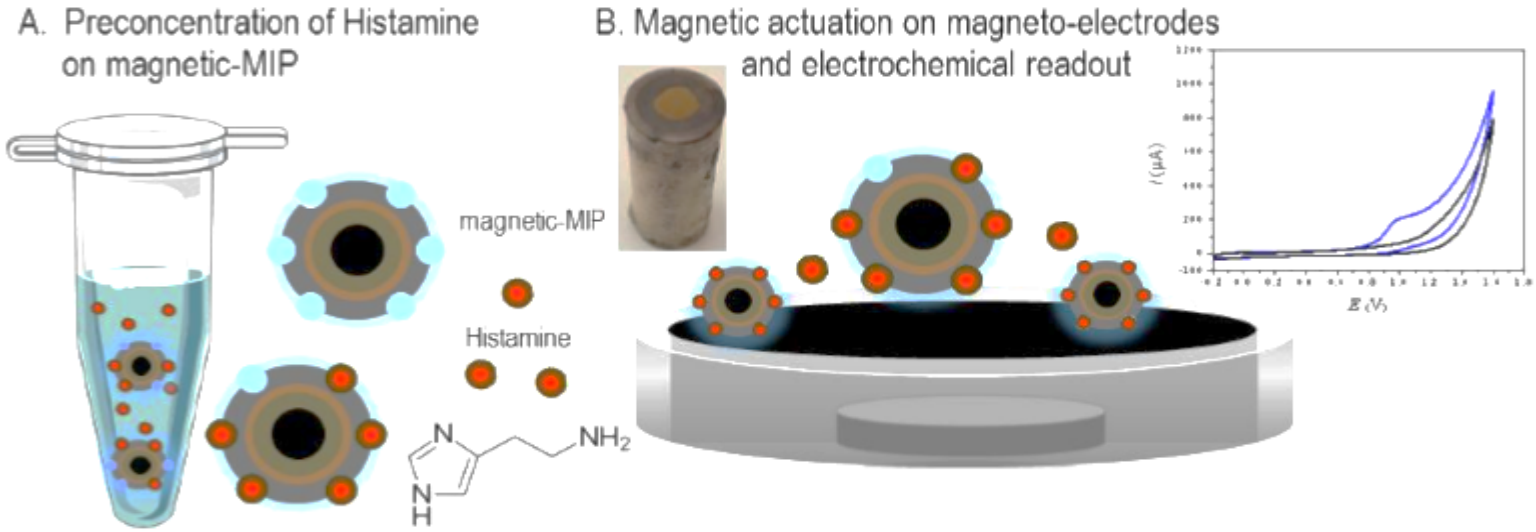

Fig. 1. Schematic procedure for the electrochemical sensing of histamine preconcentrated on magnetic-MIP by magnetic actuation on m-GEC electrodes.

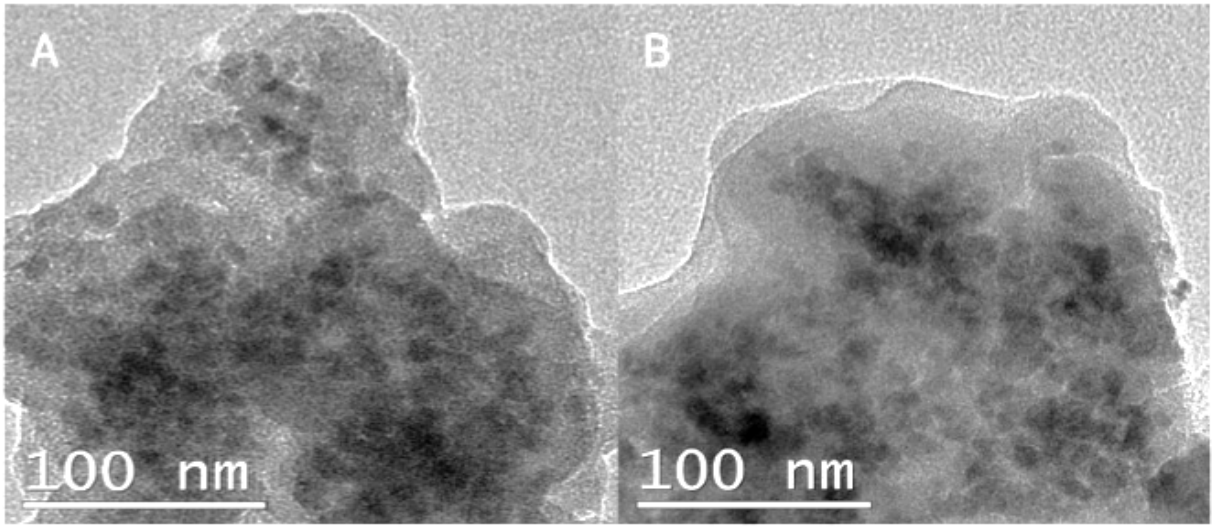

Fig. 2. Comparative study of magnetic-MIP (Panel A) and magnetic-NIP (Panel B) by transmission electron microscopy.

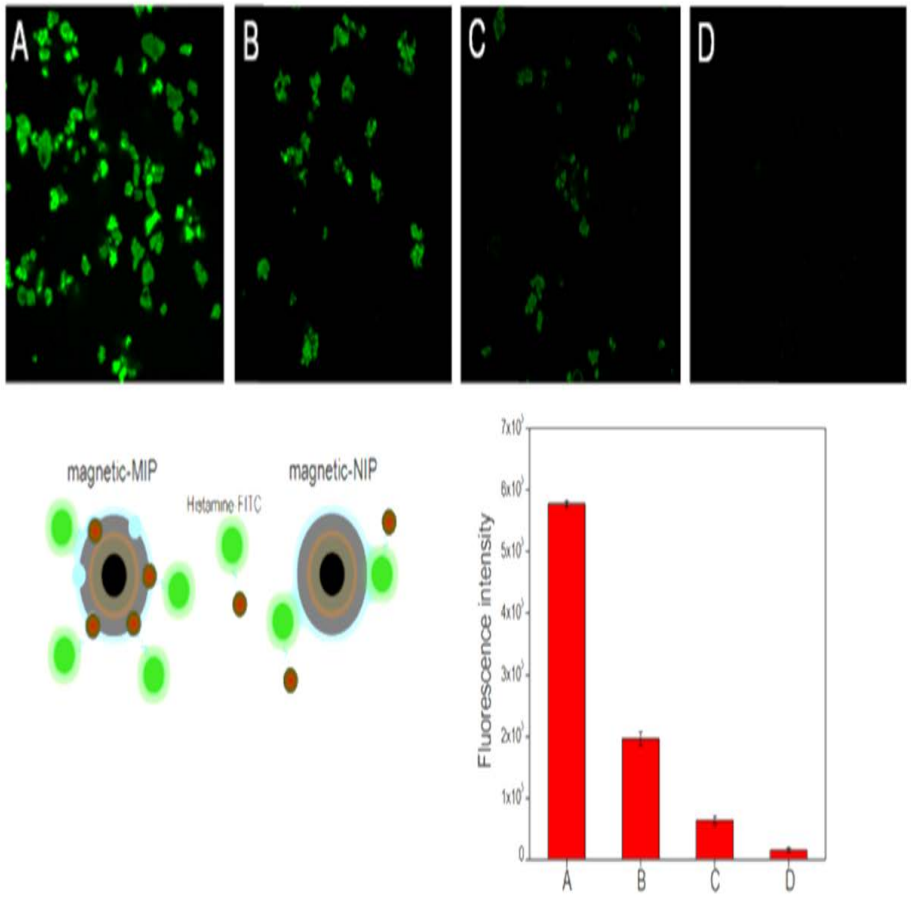

Fig. 3. Confocal microscopy for the characterization of the binding of histamine-FITC conjugate on 2-vinyl pyridine magnetic-MIP (A) and the corresponding NIP (B). Furthermore, the confocal images for methacrylic acid magnetic-MIP (C) and NIP (D) is also shown. The corresponding fluorescence intensity values at 518 nm for each of the material are also shown (n=3).

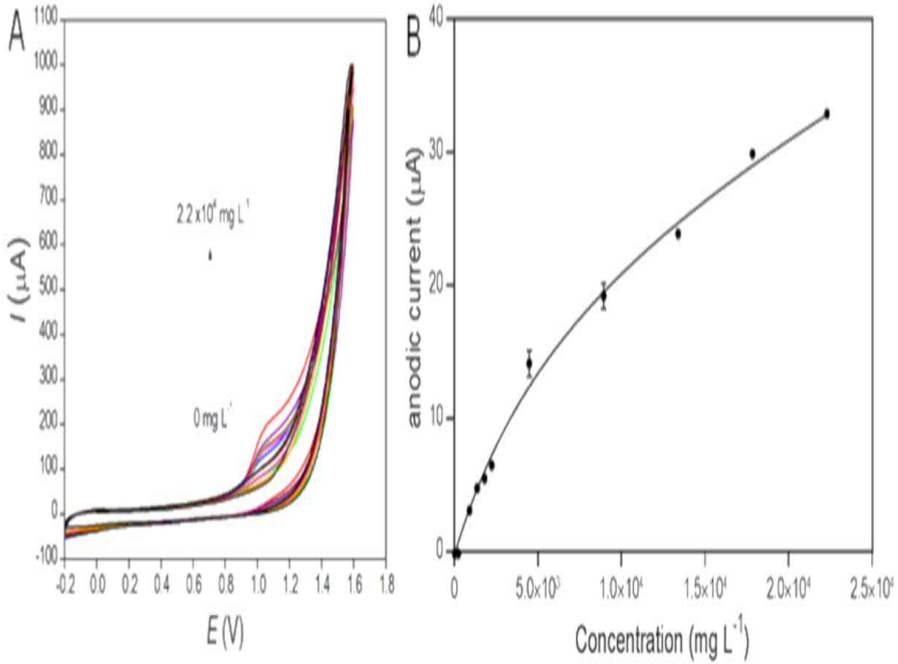

Fig. 5. Panel A. CV at different concentrations of histamine (ranging from 0 to 2.2 x 10^{4} mg L^{-1}) on a bare m-GEC electrodes, and performed by spiking 100 µL in 20 mL of PBS. Panel B. Calibration plot of the anodic current values at different concentrations of histamine (0-11.1 mg L^{-1}) on a bare m-GEC electrode in 20.0 mL of PBS. The oxidation peak current was fitted by a nonlinear regression (Two site binding hyperbola, R^{2}= 0. 9940). Error bar shows the standard deviation (n=3).

✓ From Electrochemical Biosensors to Biomimetic Sensors Based on Molecularly Imprinted Polymers in Environmental Determination of Heavy Metals[5]

- Molecularly imprinted polymers (MIPs) 기반 Inhibition-enzyme electrochemical biosensors와 biomimetic sensors들이 보고되고 있으며 중금속용 센서로는 Electro-synthesized MIPs가 독성을 평가하기 위한 biomimetic electro-chemical sensors로 보고되고 있음.

- Mmulti-template imprinting은 단일 종의 동시 검출을 센싱하기 위하여 연구되고 있으나 종 분화 능력 (speciation capability)은 충분히 나타나지 않는 문제가 있는데 효소 억제 전기 화학적 바이오 센서 (enzyme inhibition electrochemical biosensor)는 이러한 문제를 극복함.

➢ BIOSENSOR

- 중금속 측정을 위한 전기 화학적 바이오 센서와 관련된 최근의 작업이 Table 1에 요약되어 있으며 효소 시스템 (HRP, GOx, β 갈락토시다아제)에 적용된 보고가 거의 없음.

➢ BIOMIMETIC SENSORS BASED ON ELECTROSYNTHESIZED MIPS

- 아직 보고되고 있지 않거나 부분적으로 보고되고 있는 electro-synthesized MIPs (e-MIPs) 기반 중금속 전기화학센서들의 결과를 Table 2에 보고하고 있음.

- Table 1과 비교하여 Table 2는 MIP artificial receptors 기반 전기화학센서들의 높은 선택성 (selectivity), 안정성 (stability 을 보고하고 있음.

TABLE 1 | A summary of analytical characteristics of biosensors for determination of heavy metal ions based on enzyme inhibition.

Sensor	Metal Ions	Methods	Detection limit (M)[1]	Linear range (M)[1]	Tested interference[2]	Regeneration method	Stability[3]	Recovery in real samples	References
MT-MWCNT/HRP[c]	Pb^{2+}	Amperometry	7.55×10^{-9}	$2.78 \times 10^{-7} - 1.66 \times 10^{-6}$	Ca^{2+}, Mg^{2+}, Na^{+}, K^{+}	N.R.	SL: 10	96–104%[4]	Moyo et al., 2014
	Cu^{2+}		2.24×10^{-8}	$3.63 \times 10^{-7} - 1.06 \times 10^{-5}$			WL: 10		
PPy/GOx[a]	Cu^{2+}	Potentiometry	7.9×10^{-8}	$7.9 \times 10^{-8} - 1.6 \times 10^{-5}$	N.R.	Water and PBS 10–15′	SL: 8	98–101%[4]	Ayenimo and Adeloju, 2015
	Hg^{2+}		2.5×10^{-8}	$2.5 \times 10^{-8} - 5 \times 10^{-6}$					
	Pb^{2+}		2.4×10^{-8}	$1 \times 10^{-7} - 1.5 \times 10^{-5}$					
	Cd^{2+}		4.4×10^{-8}	$4 \times 10^{-8} - 6.2 \times 10^{-5}$					
PANI-co-PDTDA/HRP[a]	Cd^{2+}	DPV	7.11×10^{-12}	$0 - 8.89 \times 10^{-11}$	Fe^{2+}, Ni^{2+}, Co^{2+}, Na^{+}, SO_4^{2-}, PO_4^{3-}	N.R.	SL: 5–7	96–104%[4] 112–128%[5]	Silwana et al., 2014
	Pb^{2+}		4.52×10^{-12}	$0 - 4.82 \times 10^{-9}$					
	Hg^{2+}		3.93×10^{-12}	$0 - 4.98 \times 10^{-9}$					
N-CNTs/GOx[b]	Ag^{+}	Amperometry	1.8×10^{-9}	$2 \times 10^{-8} - 2 \times 10^{-7}$	**Cu^{2+}**; Co^{2+}	PBS	WL: 6	N.R.	Rust et al., 2015
BSA/glycerol/β-galactosidase[d]	Cd^{2+}	EIS	6.18×10^{-8}	$2.09 \times 10^{-8} - 2.09 \times 10^{-1}$	N.R.	N.R.	N.R.	95-103%[5]	Fourou et al., 2016
	Cr^{6+}	EIS	1.76×10^{-9}	$5.65 \times 10^{-10} - 5.65 \times 10^{-4}$					
	Cd^{2+}	SWV	6.76×10^{-11}	$2.09 \times 10^{-11} - 2.61 \times 10^{-1}$					
	Cr^{6+}	SWV	1.76×10^{-9}	$5.65 \times 10^{-10} - 5.65 \times 10^{-4}$					
PNR/HRP[e]	Cr^{3+}	Amperometry	0.27 μM	0.2 – 5.1 μM	Zn^{2+}, Cu^{2+}, Cd^{2+}, Co^{2+}, Ni^{2+}, Hg^{2+}, Pb^{2+}	Acetate Buffer	SL: 21	N.R.	Attar et al., 2014
	Cr^{6+}		1.6 μM	0.05 – 035 μM					

[a] *Platinum electrode (PtE).*
[b] *Glassy carbon electrode rotating disk (GC-RDE).*
[c] *Glassy carbon electrode (GCE).*
[d] *Gold electrode (AuE).*
[e] *Carbon film electrode (CFE).*
[1] *Some values have been transformed in molar concentration.*
[2] *Interferents species are in bold character.*
[3] *SL, Storage Life: days; WL, Working Life: number of consecutive measurements.*
BSA, Bovine serum albumin; DPV, Differential pulse voltammetry; EIS, Electrochemical impedance spectroscopy; GOx, Glucose oxidase; HRP, Horseradish peroxidase; MT-MWCNTs, Maize tassel-multi-walled carbon nanotubes ; N-CNTs, Nitrogen-doped carbon nanotubes; PANI-co-PDTDA, Poly(aniline-co-2,2-dithiodianiline); PNR, Poly neutral red; PPy, Poly pyrrole; SWV, Square wave voltammetry.
Range of percentage obtained by the analysis in real samples ([4] tap water, [5] river water).

TABLE 2 | A summary of analytical characteristics of ion imprinted electrosynthetized polymers (IIPs) for heavy metals determination.

Sensor	Metal Ions	Methods	Detection limit(M)[1]	Linear range(M)[1]	Tested interference[2]	Stability[3]	Recovery in real samples	References
MWCNTs/Poly Arginine[b]	Cd^{2+} Cu^{2+} Pb^{2+}	DPSV	4.94×10^{-9} 1.32×10^{-8} 2.36×10^{-9}	$1.99 \times 10^{-8} - 9.87 \times 10^{-7}$ $5.97 \times 10^{-8} - 2.95 \times 10^{-6}$ $9.75 \times 10^{-9} - 2.97 \times 10^{-7}$	Ascorbic acid, glucose, Fe^{2+}, Hg^{2+}, Zn^{2+}	SL: 45	N.R.	Roy et al., 2014
MPMBT-SiO_2[a]	Hg^{2+}	SWASV	1×10^{-10}	$1 \times 10^{-9} - 1.6 \times 10^{-7}$	Pb^{2+}, Cd^{2+}, Zn^{2+}, Cu^{2+}, Ag^{+}	SL: 40	93.1–108.7%[5]	Fu et al., 2011
PPy/EBB[a]	Cu^{2+}	DPASV Potentiometry	2×10^{-9} 1.0×10^{-8}	$3.2 \times 10^{-8} - 1.0 \times 10^{-4}$ $5 \times 10^{-8} - 1.0 \times 10^{-2}$	**Hg^{2+}, Ag^{+}**, Ni^{2+}, Co^{2+}, Cd^{2+}, Cr^{3+}, Mn^{2+}, Fe^{3+}, Pb^{2+}, Zn^{2+}	SL: 30	97.1–98.4%[5]	Zanganeh and Amini, 2008
PANI/SSA[a]	Ag^{+}	DPASV Potentiometry	2×10^{-11} 1×10^{-9}	$1 \times 10^{-10} - 1 \times 10^{-7}$, $1 \times 10^{-8} - 1 \times 10^{-4}$ $1 \times 10^{-8} - 1 \times 10^{-3}$	**Hg^{2+}**, **Cu^{2+}**, Na^{+}, K^{+}, Mg^{2+}, Ba^{2+}, Zn^{2+}, Al^{3+}, Pb^{2+}, Co^{2+}, Hg^{2+}, Cr^{3+}, Cd^{2+}, Ni^{2+}	SL: 50	92.2–96%[5]	Hashemi and Zanganeh, 2016
PMB/Gly[a]	Cu^{2+}	DPV	4.24×10^{-11}	$5 \times 10^{-10} - 3 \times 10^{-8}$	K^{+}, Na^{+}, Ca^{2+}, Mg^{2+}, Fe^{3+}, Al^{3+}, Cr^{3+}, Mn^{2+}, Hg^{2+}, Cd^{2+}, Ni^{2+}, Zn^{2+}, Co^{2+}, Pb^{2+}	N.R.	98.1%[6] 95.5%[7] 101.4%[8] 98.1–105.6%[9]	Li et al., 2015
PPy/EBB[a]	Ag^{+}	Potentiometry DPASV	6.3×10^{-9}	$1 \times 10^{-8} - 1 \times 10^{-1}$, $3 \times 10^{10} - 1 \times 10^{-7}$, $1 \times 10^{-8} - 1 \times 10^{-4}$	**Hg^{2+}**, Cd^{2+}, Cu^{2+}, Cr^{3+}, Co^{2+}, Mn^{2+}, Fe^{2+}, Fe^{3+}, Ni^{2+}, Pb^{2+}	SL: 60	98%[10]	Zanganeh and Amini, 2007
PPy/ARS[a]	Ag^{+}	Potentiometry Voltammetry	2.5×10^{-8} 4.6×10^{-10}	$5 \times 10^{-8} - 6.3 \times 10^{-3}$ $9.2 \times 10^{-10} - 2.8 \times 10^{-6}$	K^{+}, Na^{+}, **Hg^{2+}**, NH_4^{+}, Cd^{2+}, Pb^{2+}, Ba^{2+}, Zn^{2+}, Ni^{2+}, Mn^{2+}, Cu^{2+}, Al^{3+}, Cr^{3+}	N.R.	102%[4] 103%[5] 102.2%[11]	Rounaghi et al., 2015
MR/PPy[a]	Cu^{2+}	Potentiometry ASV	5.0×10^{-7} 6.5×10^{-9}	$3.9 \times 10^{-6} - 5.0 \times 10^{-2}$ $1.0 \times 10^{-8} - 1.0 \times 10^{-3}$	**Pb^{2+}**, **Hg^{2+}**, **Ag^{+}**, Ni^{2+}, Co^{2+}, Cd^{2+}, Cr^{3+}, Ba^{2+}, Fe^{3+}, Al^{3+}, K^{+}, Na^{+}	SL: 5	N.R.	Mazloum-Ardakani et al., 2013

[a] *Glassy carbon electrode (GCE).*
[b] *Gold electrode (AuE).*
[1] *Some values have been transformed in molar concentration.*
[2] *Interferents species are in bold character.*
[3] *SL, Storage Life: days*
Range of percentage recoveries obtained by the analysis in real samples ([4] tap water, [5] river water, [6] running water, [7] fruit juice, [8] rain water, [9] beer, [10] water samples, [11] waste water sample).
ASV, Anodic stripping voltammetry; ARS, Alizarin Red S; DPASV, Differential pulse anodic stripping voltammetry; DPSV, Differential pulse stripping voltammetry; DPV, Differential pulse voltammetry; EBB, Eriochrome Blue-Black B; Gly, Glycine; MPMBT, Microporous poly(2-mercaptobenzothiazole); MR, Methyl red; MWCNTs, Multi-walled carbon nanotubes; PANI, Poly aniline; PMB, Poly Methylene Blue; PPy, Poly pyrrole; SSA, 5-sulfosalicylic acid; SWASV, Square wave anodic stripping voltammetry.

참고 문헌

1. Biomimetic Tactile Sensors with Bilayer Fingerprint Ridges Demonstrating Texture Recognition, E. Choi, O. Sul, J. Lee, H. Seo, S. Kim, S. Yeom, G. Ryu, H. Yang, Y. Shin and S.-B. Lee,* Micromachines ,10(64), 2019

2. Ti-Catalyst Biomimetic Sensor for the Detection of Nitroaromatic Pollutants, A. Lemaire, P. Hapiot, F. Geneste*, Anal. Chem., 91(4), 2019

3. Electrochemical sensors based on biomimetic magnetic molecularly imprinted polymer for selective quantification of methyl green in environmental samples, S. Khan, A. Wong, M. V. B. Zanoni, M. D. P. T. Sotomayor , Materials Acience and Engineering: C, 103, 2019,

4. Biomimetic magnetic sensor for electrochemical determination of scombrotoxin in fish, A. H. A. Hassan, L. Sappia, S. L. Moura, F. H. M. Ali, W. A. Moselhy, M. d. P. T. Sotomayaor, M. L. Pividori, Talanta, 194(1), 2019

5. From Electrochemical Biosensors to Biomimetic Sensors Based on Molecularly Imprinted Polymers in Environmental Determination of Heavy Metals, C. malitesta*, S. D. Masi, E. Mazzotta, Front. Chem., 5(47), 2017